Available online at www.sciencedirect.com
SCIENCE DIRECT®
ELSEVIER
International Journal of Solids and Structures 43 (2006) 3895–3904
INTERNATIONAL JOURNAL OF SOLIDS and STRUCTURES
www.elsevier.com/locate/ijsolstr

On the stress concentration around a hole in a half-plane subject to moving contact loads

L. Afferrante *, M. Ciavarella, G. Demelio

CEMeC-PoliBA—Centre of Excellence in Computational Mechanics—Politecnico di Bari, Via Re David, 200—70124 Bari, Italy

Received 3 May 2005
Available online 1 July 2005

Abstract

We study the stress concentration due to a pore in an elastic half-plane, subject to *moving* contact loading, in the entire range of possible geometrical parameters (contact area/hole diameter, hole depth/hole diameter). Since the number of cases is very large to study with FEM even with modern machines, the use of a recent simple approximate formula due to Greenwood based on the stress field in the absence of the hole is first attempted, and compared with a full FEM analysis in sample cases. To further distillate the effects of the hole distance from the free surface and of the contact area size, the limiting cases are studied of: (i) concentrated load perpendicular to the surface and aligned with the hole centre; (ii) constant unit pressure on the top surface of the half-plane and (iii) hydrostatic load. A full investigation is then conduced for the case of Hertzian load on the surface, and it is seen that the tensile stress concentration is significantly reduced with respect to that of the concentrated load, when the contact area size is of the same order of the hole radius. Results obtained with the approximate Greenwood formula are generally accurate however only if the hole distance from the surface is greater than two times the hole radius.

Keywords: Stress concentration; Contact mechanics; Inclusions

1. Introduction

A recent method due to Greenwood (1989) suggests a simple estimate of stress concentration due to a hole, using only the stresses in the full plane in the absence of the hole. This is of particular interest in the case where the stress field induced in the absence of the hole is varying in time and is particularly complex, like in the case of moving contact loads, producing rolling contact fatigue (RCF). RCF is a subject of

* Corresponding author. Tel.: +39 0805963794; fax: +39 0805963411.
E-mail address: luciano@poliba.it (L. Afferrante).

0020-7683/$ - see front matter © 2005 Published by Elsevier Ltd.
doi:10.1016/j.ijsolstr.2005.05.003

much interest, and fatigue from stress raisers such as pores or inclusions is one of the most important causes of failure. In simpler loading conditions, the effect of pores and other defects on material resistance is relatively well known, as various empirical models exists. For example, to name one of the most well known, that developed by Murakami and Endo (1994) shows that the reduction on fatigue resistance in terms of a fatigue limit σ_w, is as a function of the defect size d with a power law similar to the classical fracture mechanics one, although weaker, $\sigma_w \approx d^{-1/6}$. However, most models refer to mainly uniaxial tension/compression loading. The case of rolling contact fatigue, vice versa, is one case with additional difficulties because of the complex stress field induced (Ekberg and Marais, 2000; Ekberg and Sotkovszki, 2001). The types of material defects occurring in railway wheels or in railway lines subject to contact loads may be various depending on the manufacturing process, for example non-metallic inclusions, such as manganese sulphide, and silicon oxide, metallic inclusions, such as aluminium oxides. As a limit and simple case, we shall only consider the case of pores. One recent attempt to study the effect of pores in the context of rolling contact fatigue of rail wheels with a complex elasto-plastic FEM analysis is for example (Kabo and Ekberg, 2002). In this paper, we shall limit our analysis to the elastic concentration, supposing this is the first step in the understanding of the complex fatigue phenomena occurring near the defects. Experimental investigations of stress concentrations were conducted for epoxy resin models containing a hole defect under the conditions of Hertzian contact by Yamamoto et al. (1981).

Turning back on Greenwood's (1989) method, it determines the stress distribution around the circumference of a circular hole in an infinite plate loaded with a generic set of loads, by relating these stresses with those around the circle in a plate without a hole

$$\sigma_\theta = 2\left(\sigma_\theta^{\mathrm{i}} - \sigma_r^{\mathrm{i}} + \sigma_0^{\mathrm{i}}\right) \tag{1}$$

where $\sigma_\theta^{\mathrm{i}}$ and σ_r^{i} are respectively the circumferential and radial stress in the plate without hole and σ_0^{i} is the mean stress around the circle (which coincides with the average stress $\bar{\sigma}_r^{\mathrm{i}}$ or $\bar{\sigma}_\theta^{\mathrm{i}}$).

In this paper, we specialize Greenwood's method to the case of Hertzian pressure distribution, as a useful tool to distillate the various effects inducing the stress concentration. A full FEM analysis, at least in the elastic regime, is available today to most users, but accurate results still require a significant computational effort, particularly if the load is moving on the surface and the full stress history is required. Vice versa, Greenwood's method only requires some simple manipulation of the contact stress field without the hole, which in most cases is available in closed form.

Further, to study the effect of the ratio of contact area size to hole size, and its distance from the surface, the limit cases of: (i) a concentrated load perpendicular to the surface and aligned with the hole centre; (ii) constant unit pressure on the top surface of the half-plane and (iii) hydrostatic load are considered. The results are then compared by using a full FEM analysis. Finally, with these limits in mind, the conclusions are clearly drawn in the case of Hertzian load on the surface.

For pores very close to the surface, the contact pressures do not follow the classical Hertzian distribution. However, this will induce a further dependence on material constants and is neglected in this paper and left for future investigations.

2. Formulation of Greenwood's method

We consider an elastic half-plane with a hole, subject to contact loading, and a polar coordinate system centred on the hole, as shown in Fig. 1. Firstly, if we consider the stress distribution in the half-plane with no hole, the initial stresses $\sigma_\theta^{\mathrm{i}}$, σ_r^{i} and $\tau_{r\theta}^{\mathrm{i}}$ on the circle $r = r_{cc}$ will be non-zero. When the hole is considered, the stresses σ_r^{f} and $\tau_{r\theta}^{\mathrm{f}}$ on the free surface of the hole are zero. Therefore, we need to find the stresses distribution ($\sigma_\theta^{\mathrm{c}}$, σ_r^{c} and $\tau_{r\theta}^{\mathrm{c}}$) in the zone $r > r_{cc}$ due to given tractions on the boundary $r = r_{cc}$, which subtracted to the initial stresses, give $\sigma_r^{\mathrm{f}} = \sigma_r^{\mathrm{i}} - \sigma_r^{\mathrm{c}} = 0$, $\tau_{r\theta}^{\mathrm{f}} = \tau_{r\theta}^{\mathrm{i}} - \tau_{r\theta}^{\mathrm{c}} = 0$ and non-zero values of σ_θ. Expanding the

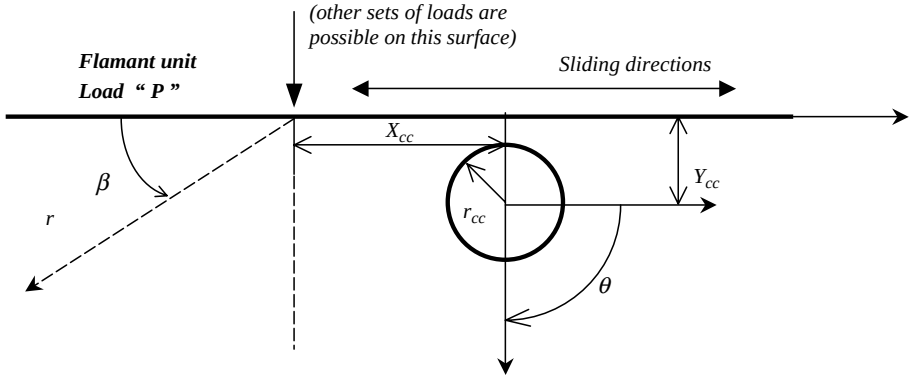

Fig. 1. System geometry and operating variables.

stresses in Fourier series around the circle $r = r_{cc}$, Greenwood (1989) found some relationships between the stress coefficient for the stresses inside the circle ($r \leqslant r_{cc}$) and those for the stresses outside the circle ($r > r_{cc}$) due to tractions around the circle, and derived Eq. (1).

In this paper, we firstly evaluate the stress field due to a contact load in the half-plane without hole by using the Flamant solution for concentrated force and the standard Hertz solution for distributed elliptical normal tractions (see Johnson, 1985).

We introduce "virtually" hole in the half-plane (with centre coordinates X_{cc} and Y_{cc} and radius r_{cc}) and evaluate the stresses on each point of the hole circumference (σ^{i}_{xx}, σ^{i}_{yy} and σ^{i}_{xy}), considering "physically" the half-plane without hole. Therefore, by standard Mohr-circle transformations, the radial stress σ^{i}_{r} can be written as:

$$\sigma^{i}_{r} = \frac{\sigma^{i}_{xx} + \sigma^{i}_{yy}}{2} + \frac{\sigma^{i}_{xx} - \sigma^{i}_{yy}}{2}\cos(2\theta) + \sigma^{i}_{xy}\sin(2\theta) \tag{2}$$

The hoop stress σ^{i}_{θ} can be obtained by substituting θ with $\theta + \pi/2$ in (1). Then, the hoop stress σ_{θ} around the hole can be evaluated by Eq. (1).

3. Special cases

3.1. Concentrated normal load (Flamant case)

A concentrated normal load P on an elastic half-plane (see Fig. 1) produces a pure radial stress field proportional to $1/r$ (see Johnson, 1985),

$$\sigma_{rr} = -\frac{2P\sin\beta}{\pi r} \tag{3}$$

and the maximum value of σ_{rr} is obtained for $\beta = \pi/2$ and X_{cc}=0 (minimum r). On the circumference of the hole, the stresses σ_{rr} can be decomposed in the stresses σ^{i}_{θ} and σ^{i}_{r} of Eq. (1). Since the average stress σ^{i}_{0} is invariant, the highest traction stress σ_{θ} around the circumference of the hole is obtained for $\theta = 270°$, where $\sigma^{i}_{\theta} = 0$ (notice that for $\theta = 270°$, $\sigma^{i}_{r} < 0$, i.e. σ^{i}_{r} is a compressive stress). For each position of load and pore depth (we fix $r_{cc} = 1$), the hoop stress σ_{θ} can be evaluated by Eq. (1). When the line load moves on the surface, every material point experiences a stress cycle. In Fig. 2 the dimensionless maximum ($\sigma_{\theta,\max} Y_{cc}/P$) and minimum ($\sigma_{\theta,\min} Y_{cc}/P$) stress on the hole circumference are plotted. In other words, each point in the

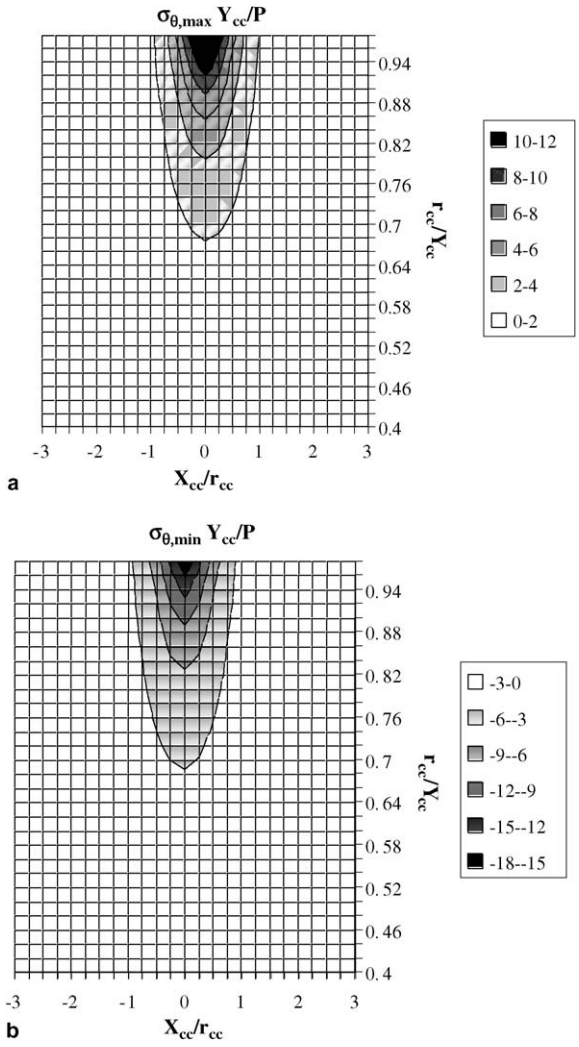

Fig. 2. (a) Maximum dimensionless hoop stress (traction) $\sigma_{\theta,\max} Y_{cc}/P$ on the circumference hole. (b) Minimum dimensionless hoop stress (compression) $\sigma_{\theta,\min} Y_{cc}/P$ on the circumference hole.

diagram represents one particular case of position of the load and depth of the hole. Notice that the y-axis increases upward (so that when $r_{cc}/Y_{cc} = 1$ we have the limit case of a hole just touching the surface, whereas lower values indicate deeper holes, hence following more naturally the fact that lower values correspond to "deeper" holes). For each given point, the contour plot gives the maximum or the minimum value of the stress reached somewhere around the circumference of the hole, for this case. Clearly, if one considers a fixed value on the vertical axes r_{cc}/Y_{cc}, one can follow an entire cycle, since the maximum value of the stress anywhere in the circumference of the hole is given at that level.

With these considerations in mind, the above figures confirm that the maximum and minimum values of $\sigma_{\theta,\max} Y_{cc}/P$ and $\sigma_{\theta,\min} Y_{cc}/P$, respectively, are reached for the centred load ($X_{cc} = 0$) and by increasing the hole depth the hoop stress cycle becomes more uniform and the $\sigma_\theta Y_{cc}/P$ distribution around the hole becomes more uniform in agreement with previous results (Yamamoto et al., 1981). For this reason, the fol-

lowing results in this paragraph are concerned with the load perpendicular to the surface and aligned with the hole centre.

Fig. 3a shows the comparison between the theoretical Greenwood results and the numerical ones (obtained with a FEM analysis refined up to 30 000 elements) in terms of the dimensionless maximum tensile hoop stress $\sigma_{\theta,\max} Y_{cc}/P$ of the hole vs r_{cc}/Y_{cc}. FEM and Greenwood results are in agreement (error lower than 30%) for $r_{cc}/Y_{cc} < 0.5$ (i.e. for a depth of the hole at least 2 times larger than radius), whereas for $r_{cc}/Y_{cc} > 0.5$ the difference between FEM and Greenwood results quickly increases (for $r_{cc}/Y_{cc} \approx 0.7$ the FEM maximum tensile hoop stress is twice larger than that predicted by the Greenwood method).

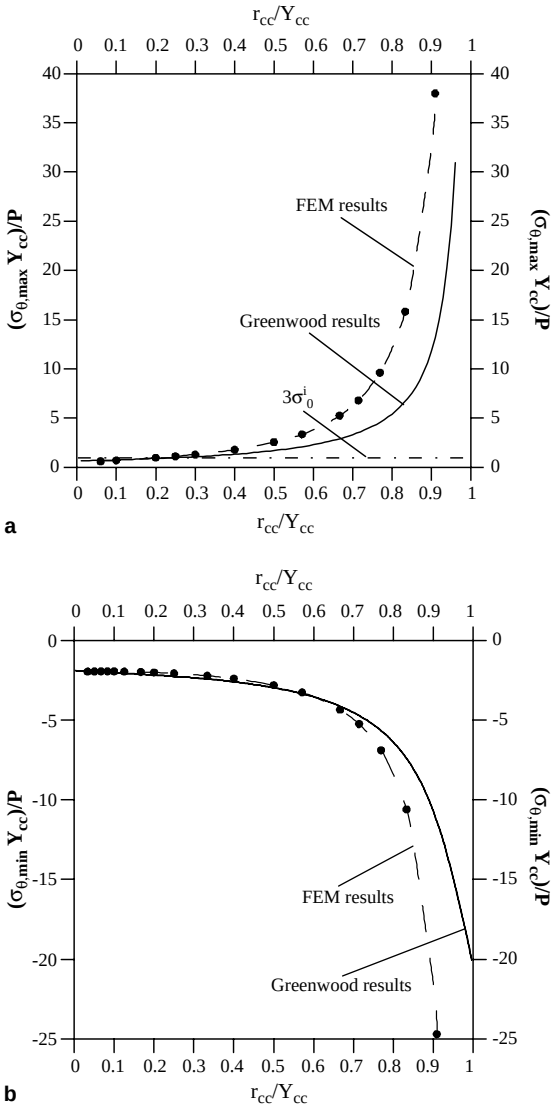

Fig. 3. (a) Comparison between FEM and Greenwood results: dimensionless tensile hoop stress $\sigma_{\theta,\max} Y_{cc}/P$. (b) Comparison between FEM and Greenwood results: dimensionless compressive hoop stress $\sigma_{\theta,\min} Y_{cc}/P$.

Both analyses (FEM and theoretical) confirm that the maximum tensile hoop stress on the pore is reached for an angle $\theta = 270°$ (see Fig. 1), i.e. on the "north pole" of the hole. Better agreement between numerical and Greenwood data is found on the maximum compressive hoop stress on the pore (similar results are obtained even up to $r_{cc}/Y_{cc} = 0.7$), as shown in Fig. 3b, where the dimensionless parameter $\sigma_{\theta,\min} Y_{cc}/P$ is plotted against r_{cc}/Y_{cc}. However, FEM and Greenwood analysis give different angular positions of the maximum compressive hoop stress. In fact, for Greenwood analysis the maximum compressive stress is always reached at $\theta = \pi$ (see Fig. 1), whereas for FEM analysis such position changes with the hole depth, moving from the equatorial position towards the "north pole", as the hole moves to the top surface.

3.2. Uniform uniaxial load and hydrostatic load

If we consider the limit case of a contact area very large with respect to the hole radius, neglecting the transversal direction effects, we can imagine that the hole becomes immersed in an otherwise uniaxial load. As shown by Greenwood (1989), if we introduce a hole in a plate in uniaxial compression and take $\theta = 270°$ (the angular reference is as in Fig. 1) to be the compression direction, Eq. (1) gives the following well-known hoop stresses (see Timoshenko and Goodier, 1951):

$$\sigma_\theta^{\mathrm{f}} = -T_0[1 - 2\cos[2(\theta + \pi/2)]] \tag{4}$$

with the typical result: $\sigma_\theta = +T_0$ if $\theta = \pi/2, 3\pi/2$ and $\sigma_\theta = -3T_0$ if $\theta = 0, \pi$.

However, we expect that the stress parallel to the surface will be compressive and it will be equal to the pressure next to the centre of the contact. Therefore, a better approximation of the limit case with very small hole close to the surface can be obtained by considering the half-plane loaded by hydrostatic state of stress.

If we apply Greenwood Eq. (1) to the hydrostatic load, the maximum compressive stress (achieved on the "north pole" of the hole) can be obtained ($\sigma_\theta/T_0 = -2$) by superposing the results of the case of plate loaded by uniaxial compression in both directions ($\sigma_\theta/T_0 = -3$ and $\sigma_\theta/T_0 = +1$).

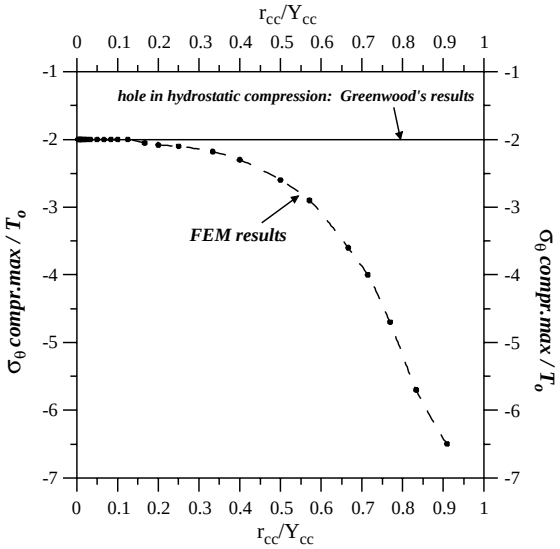

Fig. 4. Comparison between FEM and Greenwood results: maximum dimensionless compressive stress σ_θ/T_0 (hydrostatic load).

Fig. 4 shows that the agreement between Greenwood and FEM results is good up to $r_{cc}/Y_{cc} = 0.5$ (error lower than 25%). However, these stresses are negative (compressive) and hence the effect of the pore would be negligible or even *beneficial* for the fatigue strength of the material! Therefore, we are not really interested in accuracy in this limit case.

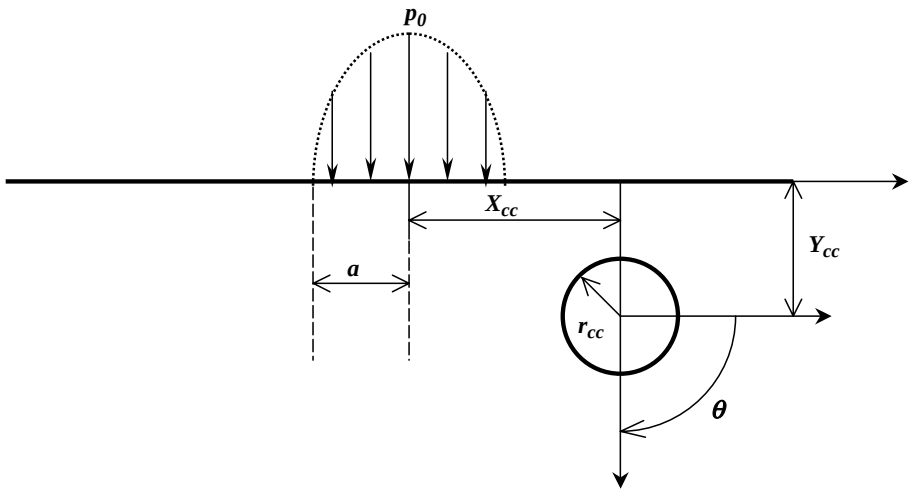

Fig. 5. System geometry and operating variables for a hole in a plate subject to a Hertzian load.

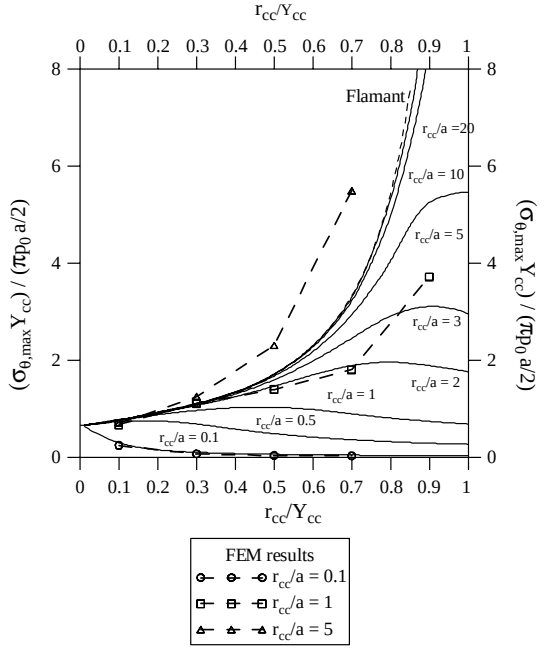

Fig. 6. Comparison between FEM and Greenwood results: dimensionless tensile hoop stress $\hat{\sigma}_\theta = (\sigma_{\theta,\max} Y_{cc})/(\pi p_0 a/2)$.

3.3. Hertzian load

The case of a concentrated normal load P on an elastic half-plane can be finally considered as the limit case of the most general Hertzian problem when the loaded area is very small with respect to the hole radius, and for this case, we have seen that the agreement between Greenwood and FEM results is good up to $r_{cc}/Y_{cc} = 0.5$ (error lower than 30%). Turning to the opposite limit case, i.e. when the Hertzian loaded area is very large with respect to the hole radius, this can be assimilated to the case of a plate loaded by a hydrostatic load. However, Hertzian stresses really approach this hydrostatic limit case only if the hole is next to surface, and in this case we are not really interested in the order of the error since the stresses would be

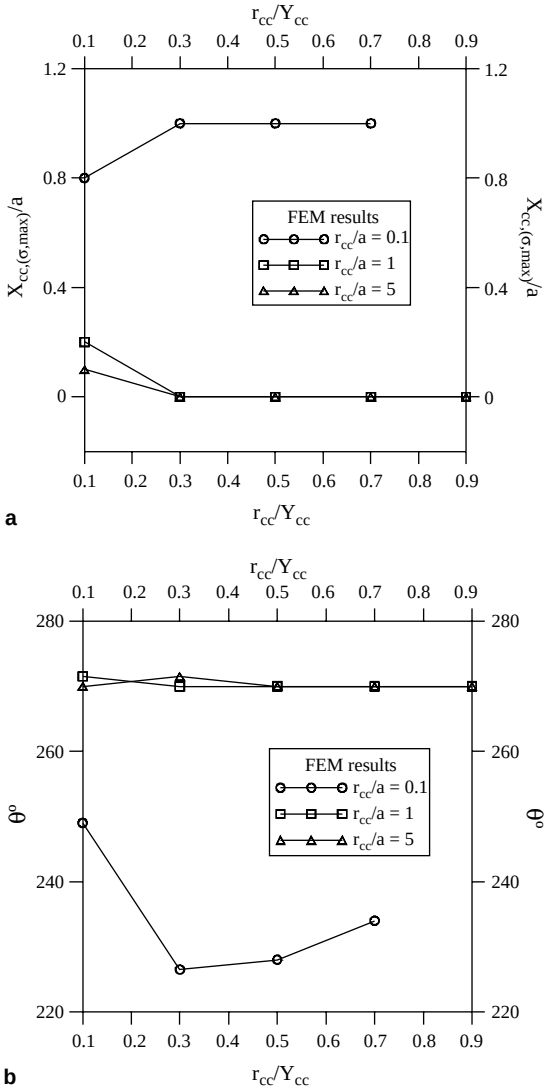

Fig. 7. (a) Load position on the surface for which the maximum hoop stress on the hole is obtained (FEM results); (b) angular positions on the hole for which the maximum hoop stress is obtained (FEM results).

compressive. Hence, we need a complete investigation to decide for which depth the agreement between Greenwood and FEM results is good, in terms of r_{cc}/Y_{cc} and r_{cc}/a.

Hence, in this section we analyse the intermediate situations of Hertzian load sketched in Fig. 5. In Fig. 6 the dependence of the dimensionless tensile hoop stresses, $\hat{\sigma}_\theta = \frac{\sigma_{\theta,\max} Y_{cc}}{\pi p_0 a/2}$, on the dimensionless parameter r_{cc}/Y_{cc} spanning the entire possible range from 0 to 1, for different values of r_{cc}/a is shown. The maximum tensile stress $\sigma_{\theta,\max}$ is obtained for distributed elliptical normal load moving on the surface. In other words, for each position j of the load the maximum hoop stress $\sigma^j_{\theta,\max}$ is evaluated, then $\sigma_{\theta,\,\max}$ is the maximum of the stresses $\sigma^j_{\theta,\max}$. Notice that for high values of r_{cc}/a ($r_{cc}/a > 20$) the Flamant solution is approached.

A good agreement with numerical results is found generally when the ratio r_{cc}/Y_{cc} is less than 0.5. Notice that in terms of stress concentration, the highest values are for larger ratios r_{cc}/a.

The most important conclusion is that, with respect to the Flamant results, the Hertz case seems to induce *much smaller stress concentration for the same depth*, although this effect is overestimated with the Greenwood method. In fact, for very small r_{cc}/a ($r_{cc}/a = 0.1$), the stress concentration *decreases* with increasing r_{cc}/Y_{cc}, instead of increasing as it does in Flamant. At higher r_{cc}/a (r_{cc}/a around 0.5) the stress concentration shows a maximum which moves to higher r_{cc}/Y_{cc} when the ratios r_{cc}/a grows. FEM results show that some of this decrease at high r_{cc}/a and r_{cc}/Y_{cc} is not real, but clearly for not too high r_{cc}/Y_{cc} and not too high r_{cc}/a interesting reductions of stress concentrations are obtained.

In Fig. 7a the load position on the surface for which the maximum hoop stress on the hole is obtained is plotted versus the parameter r_{cc}/Y_{cc} for different ratios r_{cc}/a. Symmetric load positions with respect to the hole centre yield identical results and when r_{cc}/a increases, the maximum hoop stress is obtained for centred load as in the Flamant case. However, for small r_{cc}/a, the maximum stress is not reached in a symmetrical configuration, and this requires additional computational effort.

Fig. 7b shows the angular positions on the hole for which the maximum hoop stress is obtained. When the contact area reduces with respect to the hole radius, the maximum concentration moves to the "north pole" of the pore ($\theta = 270°$).

Turning back to the evaluation of the error, in Fig. 8 the minimum ratio r_{cc}/Y_{cc} to have an error lower than 30% is plotted as a function of r_{cc}/a. This permits to rapidly verify that for $r_{cc}/a > 1$, the error between FEM and Greenwood are not too large for $r_{cc}/Y_{cc} < 0.5$, i.e. a hole depth greater than two times the hole radius.

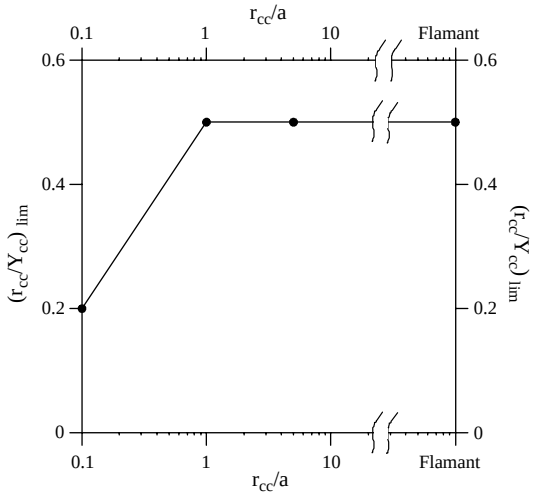

Fig. 8. Limit value of r_{cc}/Y_{cc} for which the difference between Greenwood and FEM results is less than 30%.

4. Conclusions

The stress concentration due to a hole beneath a Hertzian pressure distribution on a half-plane is studied both by means of both an approximate formula suggested by Greenwood, and a much more computationally demanding full FEM analysis. Greenwood's formula assumes the effect of the hole to be dominant with respect to the effect of the free surface. The magnitude and the location of stress concentration vary with the distance between the load and the hole. For a general Hertzian problem, a good agreement (error lower than 30%) with numerical results is found when $r_{cc}/Y_{cc} < 0.5$ i.e. a hole depth greater than twice the hole radius. When the hole radius becomes very small with respect to the contact area ($r_{cc}/a < 1$), the limit of accuracy may require deeper holes.

In terms of stress concentration, the most important conclusion is that, with respect to the Flamant results, the Hertz case seems to induce much *smaller* stress concentration for the same depth. The Greenwood formula tends to overestimate this reduction. A full FEM analysis shows that only for very small r_{cc}/a (of the order of 0.1) the stress concentration *decreases* with increasing r_{cc}/Y_{cc}, instead of increasing as it does in Flamant. At higher r_{cc}/a (r_{cc}/a around 0.5) the stress concentration shows a maximum which moves to higher r_{cc}/Y_{cc} when the ratios r_{cc}/a grows.

References

Ekberg, A., Marais, J., 2000. Effects of imperfections on fatigue initiation in railway wheels, IMechE. J. Rail Rapid Trans. 214, 45–54.

Ekberg, A., Sotkovszki, P., 2001. Anisotropy and rolling contact fatigue of railway wheels. Int. J. Fatigue 23, 29–43.

Greenwood, J.A., 1989. Exact formulae for stresses around circular holes and inclusions. Int. J. Mech. Sci. 31 (3), 219–227.

Johnson, K.L., 1985. Contact Mechanics. Cambridge University Press, Cambridge.

Kabo, Elena, Ekberg, Anders, 2002. Fatigue initiation in railway wheels—a numerical study of the influence of defects. Wear 253 (1–2), 26–34.

Murakami, Y., Endo, M., 1994. Effects of defects, inclusions and inhomogeneities on fatigue strength. Int. J. Fatigue 16, 163–182.

Timoshenko, S., Goodier, N., 1951. Theory of Elasticity. McGraw-Hill, New York.

Yamamoto, T., Eguchi, M., Murayama, K., 1981. Stress concentration in the vicinity of a hole defect under conditions of Hertzian contact. NASA Center for AeroSpace Information (CASI)—ASLE PREPRINT 81-LC-6B-2; Lubrication Conference, New Orleans, LA, October 5–7, 1981, October 1, 1981.